Larrosa, N. O., & Ainsworth, R. A. (2017). A transferability approach for reducing excessive conservatism in fracture assessments. *Engineering Fracture Mechanics*, *174*, 54-63. https://doi.org/10.1016/j.engfracmech.2016.11.011

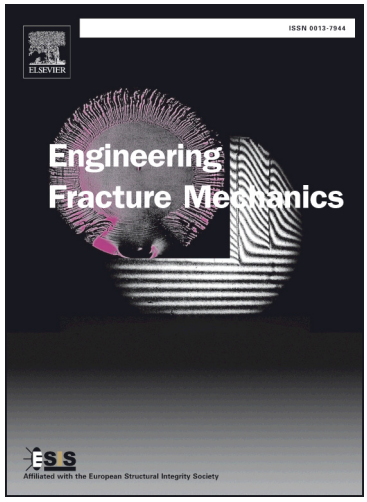

A transferability approach for reducing excessive conservatism in fracture assessments

N.O. Larrosa, R.A. Ainsworth

PII: S0013-7944(16)30594-X
DOI: http://dx.doi.org/10.1016/j.engfracmech.2016.11.011
Reference: EFM 5315

To appear in: *Engineering Fracture Mechanics*

Received Date: 22 September 2016
Revised Date: 8 November 2016
Accepted Date: 9 November 2016

Please cite this article as: Larrosa, N.O., Ainsworth, R.A., A transferability approach for reducing excessive conservatism in fracture assessments, *Engineering Fracture Mechanics* (2016), doi: http://dx.doi.org/10.1016/j.engfracmech.2016.11.011

A TRANSFERABILITY APPROACH FOR REDUCING EXCESSIVE CONSERVATISM IN FRACTURE ASSESSMENTS.

N.O. Larrosa[1] and R. A. Ainsworth[2]

[1] School of Materials, The University of Manchester, Manchester M13 9PL, UK
[2] School of Mechanical, Aerospace & Civil Engineering, The University of Manchester, Manchester M13 9PL, UK

ABSTRACT. *A source of uncertainty and conservatism in structural integrity assessments is the value of fracture toughness (K_{mat}) that is used. For conservative results, the value of K_{mat} is commonly derived from deeply cracked specimens, such as standard compact tension specimens, C(T). High constraint conditions near the crack tip are ensured and this corresponds to lower-bound toughness values independent of specimen size and geometry. However, the local stress fields in single edge notched tension, SE(T), specimens and pipes, for example, are known to be less severe than those at the tip of a deep sharp crack, resulting in an increased capacity to sustain load and higher toughness. Similar behaviour is expected when assessing non-sharp defects (e.g., pits, gouges, dents). The constraint loss or the notch effect produce a relaxation in the triaxial stress field in comparison to the severe stress fields present at deeply sharp cracked specimens. A methodology providing a simple procedure to evaluate the suitability of the use of a higher fracture toughness to reduce excessive conservatism is then required. This study uses a two-parameter fracture mechanics approach (J-Q) to quantify the level of constraint in a component (e.g. a pipe with a surface crack) and in fracture test specimens, i.e. single edge tension [SE(T]), standard compact tension [C(T)] and notched compact tension [C(T)$^{\rho}$] specimens. The ability of the structure to resist fracture is given by the fracture toughness of the test specimen with a similar J-Q response. Fracture toughness values for different specimens have been obtained from tearing resistance curves (J-R curves) constructed by means of a virtual testing framework. The proposed engineering approach is used as a platform to perform more accurate fracture assessments by the use of a ductile fracture model that informs a classical fracture mechanics approach (J-Q) by incorporating more fundamental understanding of the driving forces and the role of the geometry and loading conditions.*

Keywords: Local approach; J-Q fracture mechanics; initiation toughness; constraint; notch effect.

INTRODUCTION

In structural integrity assessments of defective components, the fracture toughness value used to determine the onset of fracture, K_{mat}, is commonly derived from deeply cracked specimens with almost square ligaments under bending, using recommended testing standards and validity criteria (e.g. ASTM E1820 [1] and ESIS-P2 [2]). These are designed to ensure high stress triaxiality, referred to as high constraint conditions, near the crack tip that correspond to lower-bound toughness values independent of specimen size and geometry.

In practical applications, there exist cases in which constraint conditions at a defect can be demonstrated to be lower than in deeply cracked bend specimens. For example, in the Oil and

Gas (O&G) industry, during installation, regions of pipeline girth welds are predominantly loaded in tension even if the pipe is globally subjected to bending. The flaw sizes of interest are usually controlled by the weld pass height and are therefore relatively small, typically 2-6 mm in height [3]. Both loading in tension and shallow notches result in reduced crack tip constraint in the component compared to the deeply notched bend specimens.

Furthermore, there is experimental evidence for panels loaded in tension which shows that the lower constraint levels around the crack tip lead to higher resistance to fracture than would be deduced from assessments based on a fracture toughness value obtained from standard bend specimens [4]. As a result, in these cases, the material capacity to withstand load is underestimated and it would be useful to perform assessments with a fracture resistance value obtained from a test specimen with a crack tip constraint condition similar to that in the actual component [5].

Materials can exhibit an increase in fracture toughness with change of loading mode from bending to tension and/or a change from deep to shallow cracked specimen geometry for both cleavage and ductile fracture modes. Although fitness-for-service codes generally require assessments based on a lower bound fracture toughness, R6[6] and BS 7910[7], for example, include assessment procedures which incorporate recommendations for toughness constraint correction. These assess the constraint loss in a component based on the elastic T-stress or the normalised opening stress Q, and also require information defining the material fracture toughness sensitivity to constraint.

In this paper, attention is focussed on ductile crack propagation behaviour (microvoid growth and coalescence). A ductile fracture simulation approach which treats material ductility as a function of stress triaxiality has been implemented in previous work [8,9] to evaluate the fracture resistance curves (J-R) for different test specimens. Although these procedures are useful tools to evaluate fracture resistance for structural components, the development and calibration of the finite element assessment (FEA) model requires extensive expertise and the application of the procedures becomes prohibitive for routine assessments. A simplified framework, which captures the increase in fracture toughness without the need for detailed analysis, is then of interest for more rapid assessments.

Two-parameter fracture mechanics which captures the load magnitude through one parameter (usually J) and the degree of stress triaxiality through a second parameter has been developed in recent years. For example, the J–Q two-parameter fracture mechanics [10,11] approach has been extensively used to characterize elastic–plastic crack front fields. The parameter Q characterizes the degree of crack tip constraint, by quantifying the level of deviation of stress/strain fields from reference fields which are characterized by high constraint.

In the work reported here, the J-Q two-parameter characterisation approach is investigated by comparing the constraint conditions of a pipe under different loading modes with those observed in high constraint compact tension, C(T), and low constraint single edge notched, SE(T), specimens. The aim is to examine whether the use of a low constraint fracture toughness value can be supported by comparing the level of constraint (Q) of a crack in a pipe with that in the SE(T) specimen, at the same applied driving force (J). An example of the use of the proposed approach to bound the fracture toughness used in a structural integrity assessment of a component to that of a specimen with a similar crack tip constraint condition given by the J-Q characterisation is shown for a pipe with a shallow circumferential crack for two different loading conditions (internal pressure and global bending).

THEORETICAL BACKGROUND

Two parameter J-Q theory

In small-scale yielding, there is always a zone of single parameter (*K*, *J*, CTOD) dominance. The crack-tip conditions are fully defined by the single parameter, whose value depends on load, crack size and geometry. The situation changes as plasticity develops when the loss of constraint becomes apparent (e.g., fully plastic response or shallow cracks), and single parameter dominance does not hold. Under these circumstances, the stresses near the crack tip are not given by the single parameter but also depend on the configuration (loading type, geometry and material properties). In low constraint geometries the near tip stress triaxiality can be significantly lower than the high constraint J-dominant state.

The *J-Q* approach to elastic-plastic fracture mechanics was introduced to remove some of the conservatism inherent in the single parameter approach based on the J integral. The following equation provides an approximate description of the near tip stress field, σ_{ij}, over physically significant distances [10,11]:

$$\sigma_{ij} = \sigma_{ij}^{ref} + Q\sigma_0\delta_{ij} \tag{1}$$

where δ_{ij} is the Kronecker delta, σ_0 is the yield stress and σ_{ij}^{ref} is a reference field, often taken as the HRR field, the near crack tip fields for power-law plastic materials derived in [12,13]. Thus, the *Q*-factor quantifies the difference between the actual local stress at a certain reference location near the crack tip and the theoretical HRR-stress field and is given by:

$$Q = \frac{\sigma_{ij} - \sigma_{ij}^{ref}}{\sigma_0} \tag{2}$$

The actual stress field in a component and the HRR field in the forward sector of the crack-tip region differ by an approximately uniform hydrostatic stress independently of distance from the crack tip, for given values of *J* [10,11]. Therefore, Eq. (1) means that with the addition of the second parameter, a range of stress states can be obtained at a fixed deformation level (as characterised by *J*), differing by a hydrostatic stress (as characterised by *Q*). In practice, the stress field is more complex than Eq. (1) but this simplification has been found to apply for the region at the crack tip where $1 \le \frac{r\sigma_0}{J} \le 5$ [10,11], corresponding to the near crack tip zone where the fracture process zone (FPZ) for both cleavage and ductile fracture is active but outside the area where crack blunting becomes significant. Negative *Q* values indicate lower constraint conditions compared to the reference field and positive *Q* values correspond to higher constraint conditions.

A local approach to ductile fracture

An alternative framework for constraint analyses and effective fracture toughness assessment is the application of failure models, often referred to as local approaches. Local approaches couple the loading history (stress-strain) near the crack-tip region with micro-structural

features of the fracture mechanisms involved [14]. Since the fracture event is described locally, the mechanical factors affecting fracture are included in the predictions of the model. The parameters depend only on the material and not on the geometry, and this leads to improved transferability from specimens to structures than one- and two-parameter fracture mechanics methods [15].

A fracture model accounting for the ductile damage processes has been used to quantify the increased resistance of blunt defects relative to sharp ones and to demonstrate that a loss of constraint leads to an increase in the fracture properties of these materials. A phenomenological model [16] based on a stress modified fracture strain concept was used in [8,9] to construct J-R curves of notched compact tension C(T) and single edge tension SE(T).

It has been demonstrated that true fracture strain for ductile materials is strongly dependent on the level of stress triaxiality [17-19]. The model used in this study therefore uses an exponential relationship between the true fracture strain, ε_f, and stress triaxiality:

$$\varepsilon_f = \alpha \exp\left[-\gamma \frac{\sigma_m}{\sigma_e}\right] + \beta \tag{3}$$

where α, β and γ are material constants obtained by fitting test data for smooth and notched bars and the triaxiality is

$$\frac{\sigma_m}{\sigma_e} = \frac{\sigma_1 + \sigma_2 + \sigma_3}{3\sigma_e} \tag{4}$$

where σ_i (i=1-3) are principal stresses and σ_e is the von Mises stress.

Using a FE analysis technique, this model is implemented in a step-by step procedure in which at each loading step, the incremental damage, $\Delta\omega$, produced by incremental strain is assessed and added to the total damage, ω, produced in previous steps. The quantification of the incremental damage definition is performed in each finite element of the model as follows:

$$\Delta\omega_i = \frac{\Delta\varepsilon^p_{e,i}}{\varepsilon_f} \; ; \; \omega_i = \omega_{i-1} + \Delta\omega_i \tag{5}$$

where $\Delta\varepsilon^p_{e,i}$ is the equivalent plastic strain increment and ε_f is determined by the local triaxiality in the element using Eq. (3). When the total damage becomes equal to unity (ω=1), local failure is assumed to occur at the element and the initiation and propagation of a crack is simulated by reducing all the stress components to a sufficiently small value to make the contribution of the element to the resistance of the component negligible.

It should be noted that this local approach with the simulation procedure briefly summarised above has been verified by comparison with experimental data on fracture toughness test specimens and pressurised pipes, which serves as validation for this purpose. All material constants in Eq. (3) with the crack tip element size for the material and tensile properties used in this study were determined by the procedure and also verified with experimental data. More details on the numerical implementation of the model can be found in [8,9,20].

PROPOSED APPROACH: Local approach plus *J-Q* fracture mechanics

Certain combinations of load conditions and component/crack dimensions and geometry have been shown to produce crack tip elastic-plastic stress fields that are less severe than those observed in standard specimens, for the same applied SIF/J/CTOD. As a result, experimental tearing resistance curves (*J*-R curves) have been shown to be geometry and loading type dependent. In practical applications, there is evidence that the material resistance to fracture is increased in components with shallow flaws, or panels loaded in tension since these conditions lead to lower constraint around the crack tip. Thus, in structural assessments of such components, to reduce excessive conservatism, advantage can be taken by using the fracture toughness of a specimen with a similar (but higher) level of crack tip constraint. To achieve this, *J-Q* fracture mechanics is used to compare the level of crack tip constraint of the component with a series of standard and non-standard specimens.

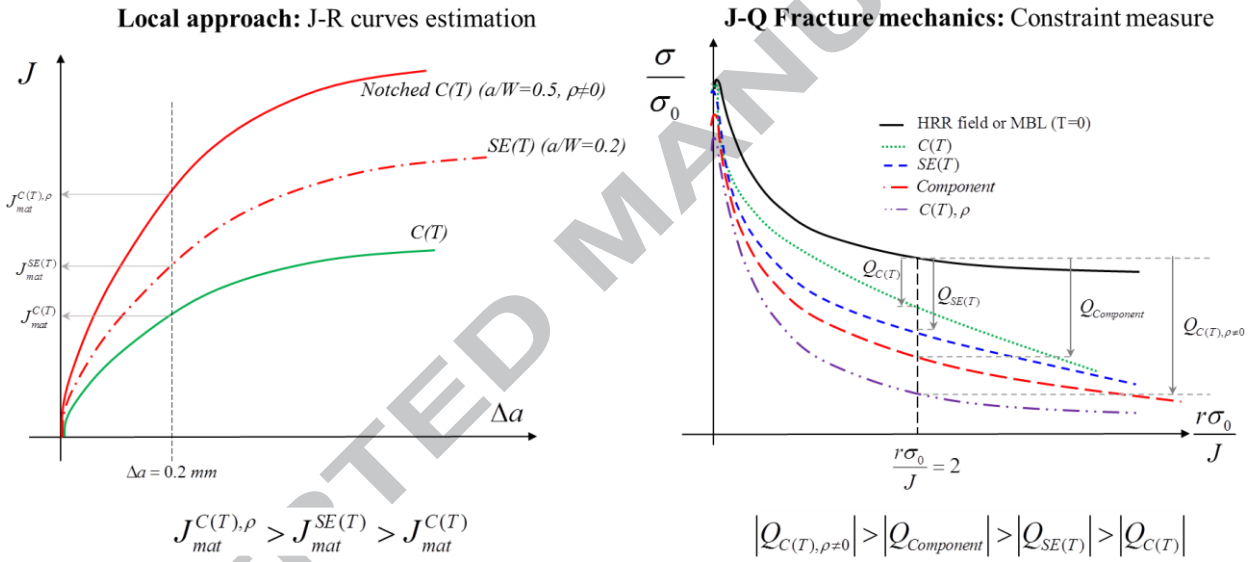

Fig. 1. Schematic illustration of the combined approaches used to support the use of a higher value of initiation toughness in structural integrity assessments.

Figure 1 shows a schematic representation of the approach proposed in this work. The local elastic-plastic stress fields in SE(T), notched C(T) specimens and a structural component, for example, are shown to be less severe than those at the tip of a deep sharp cracked C(T) specimen. The constraint measure for the component ($Q_{Component}$) limits the values of initiation toughness to those with a lower crack tip constraint, i.e. a lower capacity to sustain load. As the constraint level in the component is lower than that in the SE(T) specimen, $J_{mat}^{SE(T)}$ can be used as a conservative measure of initiation toughness, reducing the excessive conservatism when using $J_{mat}^{C(T)}$. The FE ductile fracture approach is used to evaluate the J-R curves of different standard and non-standard fracture specimens. This allows the library of J-R curves that could be used together with the *J-Q* fracture mechanics approach to be enlarged, to assess structural components.

FINITE ELEMENT ANALYSIS

A shallow cracked SE(T) specimen, two notched C(T) specimens with different crack tip radius and a deeply sharp cracked C(T) specimen were modelled by means of 3-D finite elements. The relevant dimensions of these specimens and the pipe component assessed in this work are shown in Fig. 2. The material properties used in the numerical models are for an API X65 steel used in [8,21,22], as shown in Table 1.

Table 1. Mechanical properties of API X65

Yield strength σ_0 (MPa)	Tensile strength σ_u (MPa)	Young's modulus E (GPa)	Poisson's ratio ν
464.5	563.8	210.7	0.3

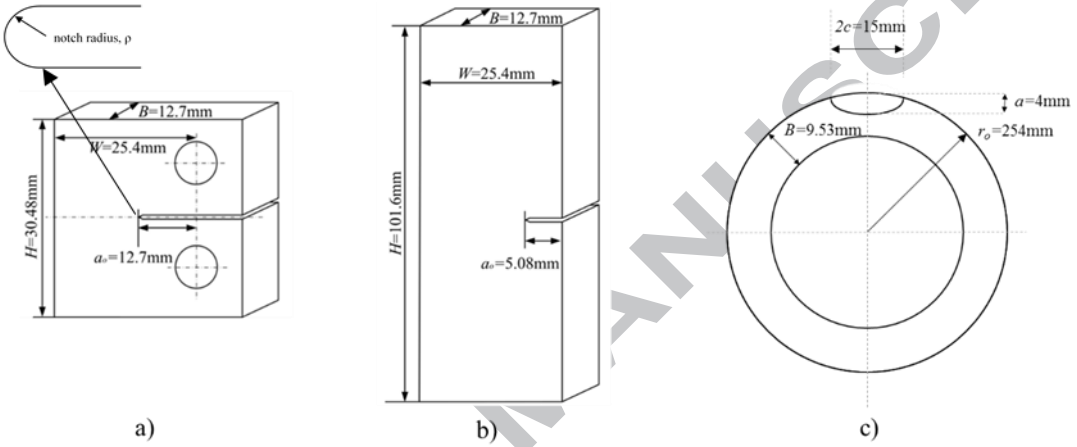

Fig. 2. Schematic illustration of fracture toughness specimens showing the dimensions: (a) C(T) specimens: sharp crack, ρ=0.3 and ρ=0.5; (b) SE(T) specimen; (c) Pipe with surface circumferential crack.

Figure 3 shows the FE models. Due to symmetric conditions of loading and geometry a quarter of C(T) and SE(T) specimens were modelled, to improve computational efficiency. One half of the pipe was modelled in order to be able to apply pure bending.

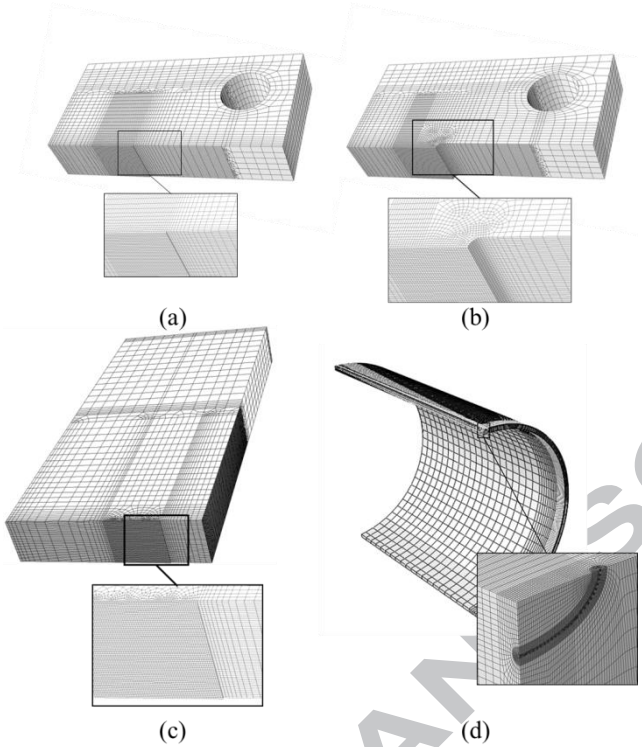

Fig. 3. Finite element models: (a) C(T) specimen; (b) notched C(T) specimen; (c) SE(T) specimen; (d) Pipe with surface circumferential crack.

In [8], it was shown that element size in the defect section affects the results for the damage accumulation process; therefore, this value must be determined by comparison with experimental results. For API X65, the element size is 0.15mm [8]. The material constants to apply the fracture criterion of Eq. (3) for API X65, based on the defined element size, are α=3.29, β= -1.54 and γ=0.01. The damage model is implemented within C3D8 hexahedron solid elements using the ABAQUS UHARD and USDFLD user-defined subroutines [23] coded in FORTRAN 90. The total numbers of elements/nodes in the FE models are from 23,366/26,016, 82,520/88,929 and 117,595/130,416 for the SE(T) specimen, deeply cracked C(T) specimen and the pipe, respectively. For the notched C(T) specimens with ρ=0.3 and ρ=0.5 mm the number of nodes/elements used was 36,927/32,290 and 37,296/33,300, respectively.

RESULTS

The numerical *J* -R curves obtained by the implementation of the damage model are shown in Fig. 4. A standard deeply cracked C(T) specimen, two notched C(T) specimen and a shallow cracked SE(T) specimen were modelled [22]. The use of the ESIS P2 procedure [2] for the estimation of the effective initiation fracture toughness is illustrated. It is observed that the local approach captures the effect of the geometry of the different specimens on the predicted *J*-R curves and that higher energy (*J*) needs to be applied to the non-standard specimens to produce the same amount of tearing (Δa) in comparison to that required by the standard C(T) specimen.

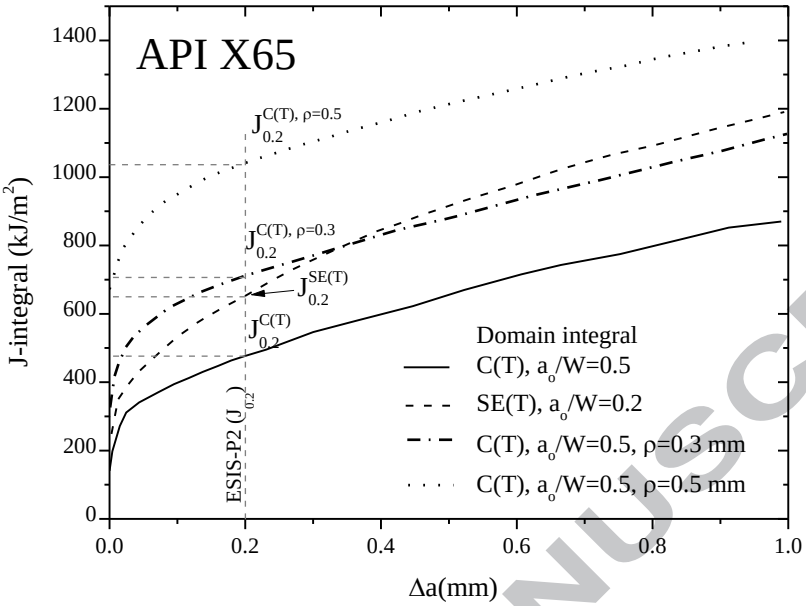

Fig. 4. J-R curves of shallow cracked SE(T) and deeply notched and sharp cracked C(T) specimens.

Next, the *J-Q* approach is used to match the constraint conditions of the different test specimens with that of a pipe component, both for the cases of applied internal pressure and pure bending, accounting for the effect of the loading mode on constraint level. In general, the value of *Q* depends on load magnitude (and therefore on *J*) as well as loading mode, being proportional to load in small-scale and large-scale yielding but weakly dependent on *J* at large loads. The values of *Q* have therefore been evaluated at applied *J* values, see Fig. 5, for the pipe at loads which cover the range of *J* at initiation in the C(T), SE(T) and notched C(T) specimens.

It can be seen from figure 5 that at these values, the stress fields in the pipe when plotted against normalised distance are weakly dependent on *J*. Hence, *Q* is also weakly dependent on *J* in this practical range. It can then be assumed that the pipe would have the same effective initiation toughness as a specimen with the same *J-Q* value. For fracture assessments where it is not possible to match the *Q* value of the pipe with that of a test specimen, the specimen with the closest higher value of Q will be a conservative choice.

The parameter *Q* is generally evaluated at a distance $r = 2J/\sigma_0$ from the crack tip and using the opening stress obtained by detailed finite element analysis, Eq. (2). The reference field in Eq. (1) is obtained from a boundary layer analysis at the same applied *K* (or *J)* with T=0, as this enables the approach to be applied to materials which do not follow the power-law form which allows the HRR field to be used as the reference field in Eq. (1).

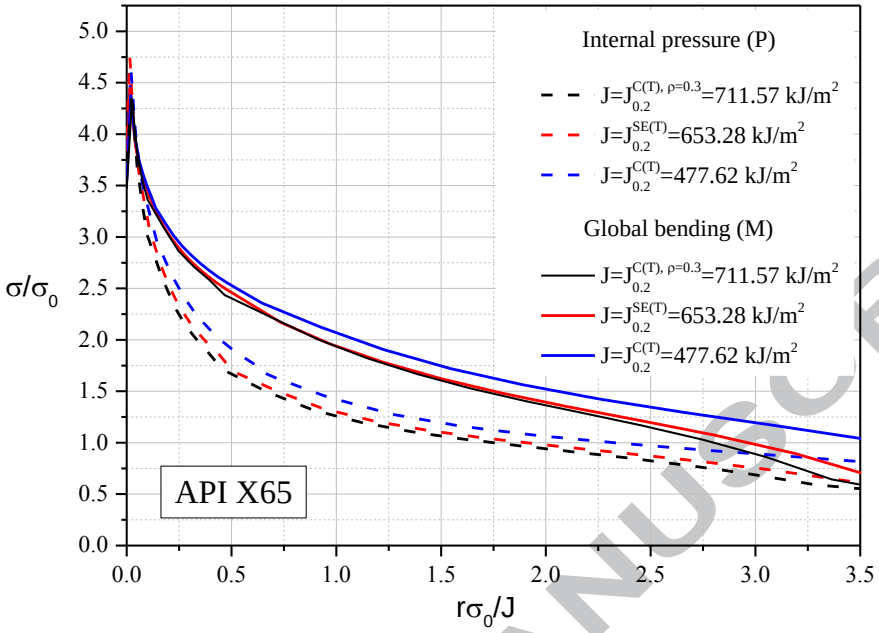

Fig. 5. Normalized crack-opening stress distribution for the pipe with different loading modes and applied J values. Note that stress fields are weakly dependent on J for this range of loads and that the difference is lower for higher J values.

Figures 6 and 7 show the normalised values of the crack tip opening mode stress field at different load levels for the test specimens, the pipe component and the modified boundary layer model. Only the relevant curves at the applied loads are shown in Figure 7, e.g. the stress field for the standard C(T) specimen is omitted from this figure. It is readily observed from the figures that the severest stress field is that of the C(T) specimen. The vertical distance from any of the curves to the MBL curve gives the value of Q. As the stress fields in the SE(T) and notched C(T) specimens are more severe than that in the pipe for both loading conditions (more negative value of Q), $J_{0.2}^{SE(T)}$, $J_{0.2}^{C(T),\rho=0.3}$ and $J_{0.2}^{C(T),\rho=0.5}$ can be used as conservative values of initiation toughness (J_{mat}) in the assessment of the pipe under both loading modes, allowing an increased loading capacity for the component in service.

Figure 8 shows the increase in pressure and bending moment that the material will be allowed to sustain by allowing the higher toughness values to be used for fracture assessment. The intercept of the horizontal lines with the curves gives the maximum applied pressure (P) and bending moment (M) for fracture assessments. The use of the proposed approach to support the use of toughness values from non-standard specimens with reduced level of constraint allows higher loads/moments to be applied conservatively. It is observed in the figure, however, that the benefit in the values of applied load/moment is less pronounced than that observed for the values of toughness. For example, only 5%, 6% and 12% increase of pressure or moment could be applied to the pipe if the toughness value used for the assessment is that of the SE(T) (37%) , the notched C(T) specimens with ρ=0.3 mm (49%) or with ρ=0.5 mm (120%), respectively. This effect is related to the steepness of the J vs P/M curves in Fig. 8.

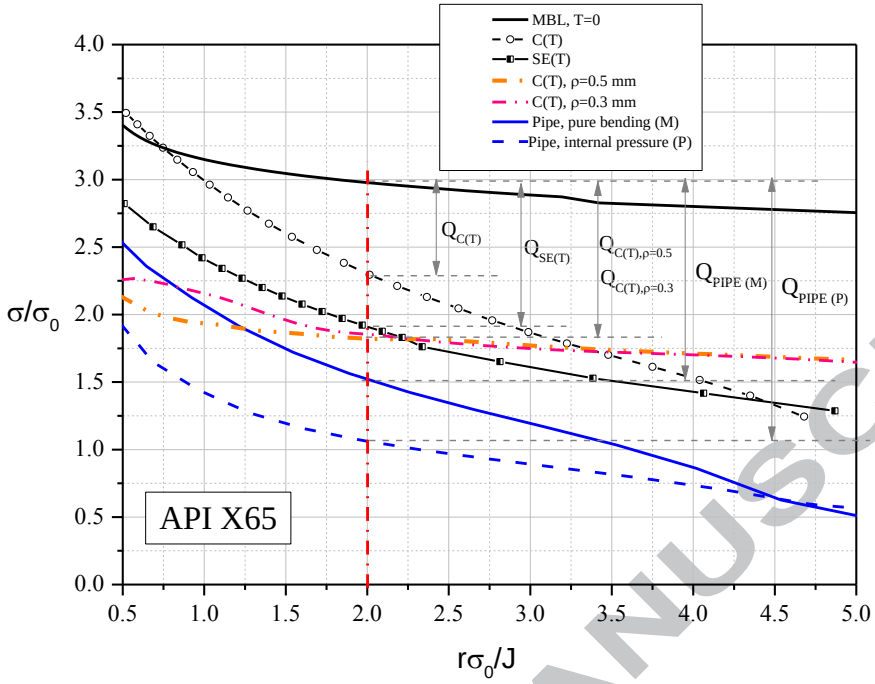

Fig. 6. Normalized crack-opening stress distribution for the different components at $J = J_{0.2}^{C(T)}$ =477.62 kJ/m^2.

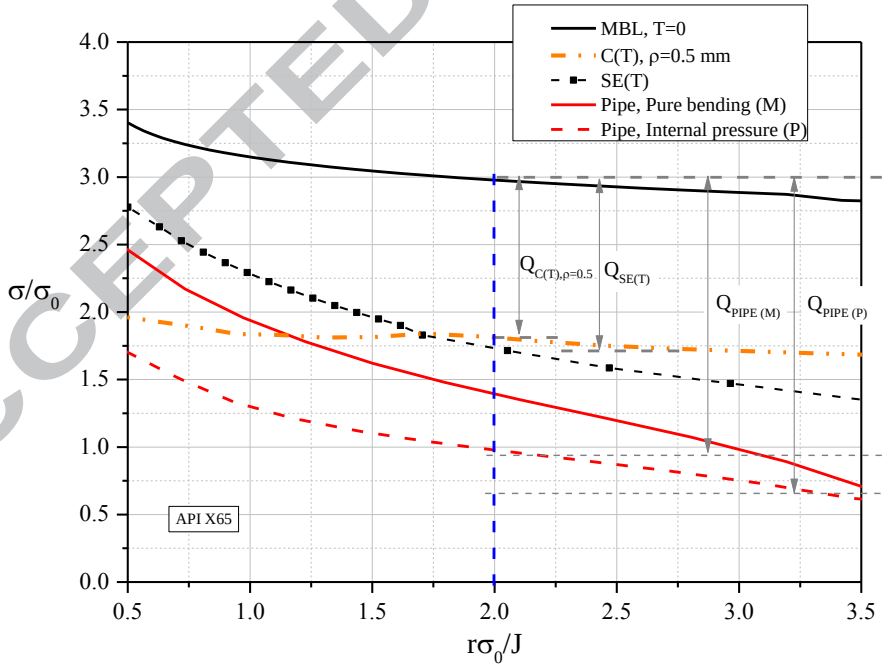

Fig. 7. Normalized crack-opening stress distribution for the different components at $J = J_{0.2}^{SE(T)}$ =653.28 kJ/m^2.

Experimental testing of full-scale pipes would be required for the approach described above to be fully validated. However, experimental validation which supports the use of detailed constraint based approaches within fitness-for-service procedures is contained in R6 [6], for a

range of geometries, and has been demonstrated for the European SINTAP procedure for some plate geometries [24]. These approaches require fracture toughness data from a range of low constraint geometries in order to estimate the fracture toughness at a constraint level matching that in the component. The approach described above is conservative compared to these detailed approaches as the fracture toughness used is from a specimen with higher constraint than the component. Therefore, the experimental validation in [6,24] also provides experimental validation for the approach proposed here.

CONCLUSIONS

Crack size, loading mode and material properties can have a strong effect on constraint conditions, affecting the material resistance to fracture.

In this work, finite element ductile fracture simulation has been used to construct J-R curves for two fracture specimens with different constraint conditions and two notched C(T) specimens. The ductile fracture model only considers a small area ahead of the crack tip (geometry independent) and couples the loading history (stress-strain) with phenomenological features of the microstructural fracture mechanism (material + loading history dependent). In addition, a Two Parameter Fracture Mechanics approach has been applied to match the constraint conditions present in a defective structural component to those present in the test specimens. By doing this, the *J-Q* approach allows an improved assessment of the fracture resistance of the component, by using the fracture resistance of the test specimen with similar constraint conditions, reducing the excessive conservatism in fracture assessments.

ACKNOWLEDGEMENTS

The authors would like to acknowledge the funding and technical support from BP through the BP International Centre for Advanced Materials (BP-ICAM) which made this research possible.

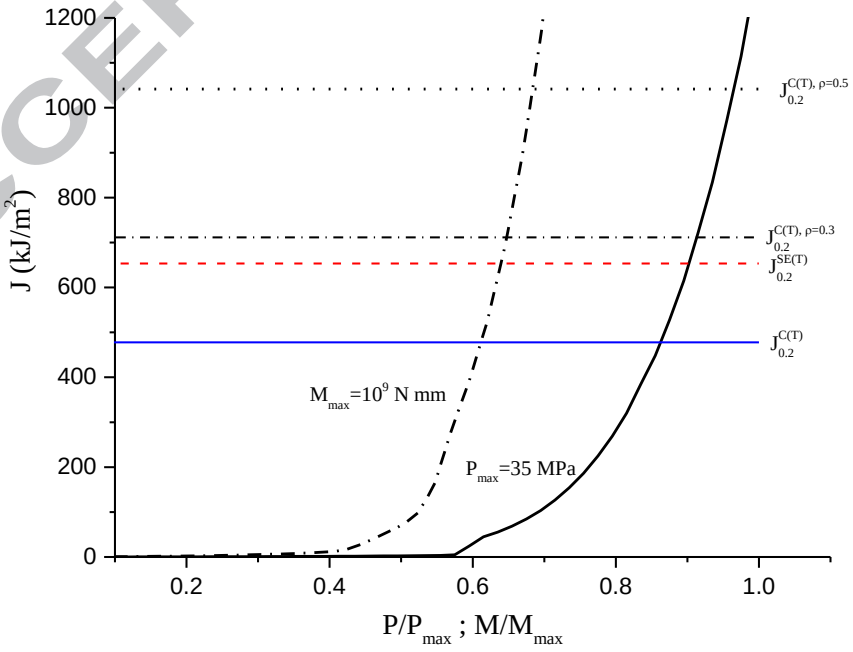

Fig. 8. J-integral values as a function of pressure (P) or bending moment (M). The horizontal lines show the

initiation toughness values for the different test specimens.

REFERENCES

1. ASTM E1820-06a, American Society for Testing and Materials. Standard Test Method for Measurement of Fracture Toughness (2001).
2. ESIS P2-92: Procedure for Determining the Fracture Behaviour of Materials (1992).
3. DNV-RP-F108, Det Norske Veritas: Fracture control for pipeline installation methods introducing cyclic plastic strain (2006).
4. Anderson T.L. Fracture Mechanics: Fundamentals and Applications. CRC press, Taylor & Francis, Boca Raton, Florida, USA (1995).
5. Cravero S. and Ruggieri C. Correlation of fracture behaviour in high pressure pipelines with axial flaws using constraint designed test specimens - Part I: Plane-strain analyses. Engineering Fracture Mechanics, 72:1344–1360 (2005).
6. R6, Revision 4, Assessment of the integrity of structures containing defects. EDF Energy, Gloucester, UK (2015).
7. BS 7910:2013. Guide to methods for assessing the acceptability of flaws in metallic structures. British Standard Institution, London, UK (2013).
8. Oh C.-S., Kim N.-H., Kim Y.-J., Baek J.-H., Kim Y.-P. and Kim, W.-S. A finite element ductile failure simulation method using stress-modified fracture strain model. Engineering Fracture Mechanics, 78, 124–137 (2011).
9. Han J.-J., Kim Y.-J. and Ainsworth, R.A. Constraint effects in ductile fracture on J-Resistance curve for full-scale cracked pipes and fracture toughness testing specimens. American Society of Mechanical Engineers, Pressure Vessels and Piping Division, Volume 5 (2014).
10. O'Dowd N.P. and Shih C.F. Family of crack-tip fields characterized by a triaxiality parameter-I: Structure of fields. Journal of the Mechanics and Physics of Solids, 39:989–1015 (1991).
11. O'Dowd N.P. and Shih C.F. Family of crack-tip fields characterized by a triaxiality parameter-II: Fracture applications. Journal of the Mechanics and Physics of Solids, 40:939–963 (1992).
12. Hutchinson J.W. Singular behaviour at the end of a tensile crack tip in a hardening material. Journal of the Mechanics and Physics of Solids, 16, 13–31 (1968).
13. Rice, J.R. and Rosengren, G.F. Plane strain deformation near a crack tip in a power-law hardening material. Journal of the Mechanics and Physics of Solids, 16, 1–12 (1968).
14. Pineau A. Development of the local approach to fracture over the past 25 years: Theory and applications. International Journal of Fracture, 138, 39–166 (2006).
15. Ruggieri C. and Dodds Jr R.H. A transferability model for brittle fracture including constraint and ductile tearing effects: A probabilistic approach. International Journal of Fracture, 79, 309–340 (1996).
16. Bao Y. Dependence of ductile crack formation in tensile tests on stress triaxiality, stress and strain ratios. Engineering Fracture Mechanics, 72, 505– 522 (2005).
17. McClintock, F.A. A criterion for ductile fracture by the growth of holes. Journal of Applied Mechanics, 35: 363–371 (1968).
18. Rice J.R. and Tracey D. M. On the ductile enlargement of voids in triaxial stress fields. Journal of the Mechanics and Physics of Solids, 17(3):201–217 (1969).
19. Hancock J.W. and Mackenzie A.C. On the mechanisms of ductile failure in high-strength steels subjected to multi-axial stress-states. Journal of the Mechanics and Physics of Solids, 24,147–160 (1976).

20. Kim Y.-J., Kim J.-S., Cho S.-M. and Kim Y.-J. 3-D constraint effects on J testing and crack tip constraint in M(T), SE(B), SE(T) and C(T) specimens: Numerical study. Engineering Fracture Mechanics, 71, 1203–1218 (2004).
21. Han J-J., Larrosa N.O., Kim Y-J., Ainsworth R.A. Blunt defect assessment in the framework of the failure assessment diagram. International Journal of Pressure Vessels and Piping, 146, 39-54 (2016).
22. Han J-J., Larrosa N.O., Ainsworth R. and Kim, Y-J. The use of SE(T) specimen fracture toughness for FFS assessment of defects in low constraint conditions. Procedia Structural Integrity, 2, Pages 1724-1737 (2016).
23. ABAQUS Version 6.13. Analysis User's Manual. Dassault Systemes Simulia Corp., Providence, RI (2013).
24. Ainsworth R.A., Sattari-Far, I., Sherry, A. H., Hooton, D.G. and Hadley, I. Methods for including constraint effects within the SINTAP procedures, Engng Fract Mech, **67** (6)**,** 563-571 (2000).

NOMENCLATURE

a	crack size
B	specimen thickness
E	elastic modulus
J	J-integral
$J_{0.2}^{C(T),\rho=\rho_1}$	J value at 0.2mm crack growth for a blunt defect with notch tip radius ρ_1
K_I	mode I stress intensity factor
P	applied pressure
P_{max}	applied pressure in the FE model
Q	Second parameter for characterising stress fields
ρ	notch root radius in C(T) specimens
W	specimen width
α, β, γ	material constants
Δa	average ductile crack growth
$\Delta\varepsilon_e^{\ p}$	incremental equivalent plastic strain
ε_f	fracture strain
σ_0	0.2% proof stress
σ_e	von Mises effective stress
σ_m / σ_e	stress triaxiality
σ_m	hydrostatic stress
$\sigma_1, \sigma_2, \sigma_3$	principal stresses
ν	Poisson's ratio
$\omega, \Delta\omega$	accumulated damage and incremental damage, respectively

Abbreviations

2-D, 3-D	two-dimensional, three-dimensional
ESIS	European Structural Integrity Society
FE	finite element
J-R	fracture resistance in terms of J versus Δa
LLD	load-line displacement
C(T)	compact tension test specimen
SE(T)	single edge tension specimen